CHEMISTRY
A EUROPEAN JOURNAL

FULL PAPER

DOI: 10.1002/chem.201203937

Encapsulation-Induced Remarkable Stability of a Hydrogen-Bonded Heterocapsule

Keisuke Ichihara,[a] Hidetoshi Kawai,[b] Yuka Togari,[a] Emi Kikuta,[a] Hitomi Kitagawa,[a] Seiji Tsuzuki,*[c] Kenji Yoza,[d] Masamichi Yamanaka,[a] and Kenji Kobayashi*[a]

Abstract: Remarkably enhanced stability of the self-assembled hydrogen-bonded heterocapsule **1·2** by the encapsulation of 1,4-bis(1-propynyl)benzene **3a** was found with $K_a = 1.14 \times 10^9\,M^{-1}$ in $CDCl_3$ and $K_{a2} = 1.59 \times 10^8\,M^{-2}$ in $CD_3OD/CDCl_3$ (10% v/v) at 298 K. The formation of **3a**@(**1·2**) was enthalpically driven ($\Delta H° < 0$ and $\Delta S° < 0$) and there was a unique inflection point in the correlation between $\Delta H°$ versus $\Delta S°$ as a function of polar solvent content. The ab initio calculations revealed that favorable guest–capsule dispersion and electrostatic interactions between the acetylenic parts (triple bonds) of **3a** and the aromatic inner space of **1·2**, as well as less structural deformation of **1·2** upon encapsulation of **3a**, play important roles in the remarkable stability of **3a**@(**1·2**).

Keywords: capsules · cavitands · host–guest systems · hydrogen bonds · supramolecular chemistry

Introduction

The binding motifs with remarkable association constants (K_a) in host–guest systems are of importance for the generation of thermodynamically stable supramolecular architectures.[1–3] Contiguous quadruple hydrogen-bonding arrays among multipoint hydrogen-bonding motifs for dimerization are quite strong and useful building blocks for this purpose.[1b,4] The construction of highly stable guest-encapsulating self-assembled hydrogen-bonded capsules, guest@capsule, is also a very important subject,[5] in which guest@capsule can be used as a modular unit.[6] Of the multipoint hydrogen-bonding motifs, the merits of using guest@capsule are that its stability can be controlled by guest molecules[7,8] and guest encapsulation endows hydrogen-bonded capsules with potential as functional materials.[7c,9]

Recently, we have reported that tetra(4-pyridyl)-cavitand **1** and tetrakis(4-hydroxyphenyl)-cavitands **2** self-assemble into a heterocapsule **1·2** in a rim-to-rim fashion through four pyridyl···phenol–hydrogen bonds in $CDCl_3$, in which one molecule of 1,4-disubstituted-benzene as a guest is encapsulated to form guest@(**1·2**), as shown in Figure 1.[10] We have explored a more appropriate guest molecule for enhancing the stability of guest@(**1·2**), the K_a value comparable to those of contiguous quadruple hydrogen-bonding arrays.[4] Herein, we report the remarkably enhanced stability of the self-assembled hydrogen-bonded heterocapsule **1·2** by the

[a] K. Ichihara, Y. Togari, E. Kikuta, H. Kitagawa, Prof. M. Yamanaka, Prof. K. Kobayashi
Department of Chemistry
Faculty of Science, Shizuoka University
836 Ohya, Suruga-ku, Shizuoka 422-8529 (Japan)
Fax: (+81) 54-238-4933
E-mail: skkobay@ipc.shizuoka.ac.jp

[b] Prof. H. Kawai
Department of Chemistry
Faculty of Science, Tokyo University of Science
Kagurazaka 1-3, Shinjuku-ku, Tokyo 162-8601 (Japan)

[c] Prof. S. Tsuzuki
Nanosystem Research Institute
National Institute of Advanced Industrial Science and Technology (AIST)
Tsukuba, Ibaraki 305-8568 (Japan)
Fax: (+81) 29-851-5426
E-mail: s.tsuzuki@aist.go.jp

[d] Dr. K. Yoza
Bruker axs, 3-9-B Moriya
Kanagawa-ku, Yokohama 221-0022 (Japan)

Supporting information for this article is available on the WWW under http://dx.doi.org/10.1002/chem.201203937.

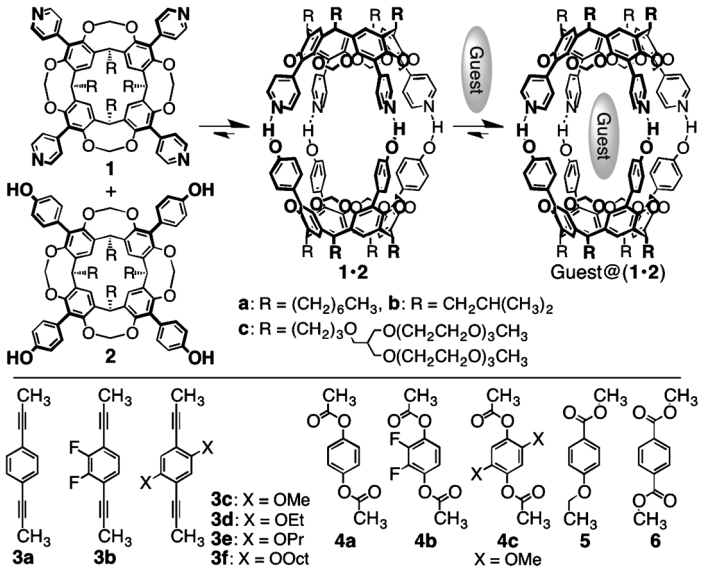

Figure 1. Self-assembly of cavitands **1** and **2** into a heterocapsule **1·2** and its guest encapsulation, and guest molecules **3**–**6**.

encapsulation of 1,4-bis(1-propynyl)benzene **3a** and its derivatives **3b–f** (Figure 1). We also describe the stability of **3a**@(**1·2**) and its unique thermodynamics in polar solvents. We further describe the ab initio calculations of **3a**@(**1·2**) to elucidate the origin of its remarkable stability, in which the acetylenic parts of **3a** are important for the **3a**–**1·2** dispersion and electrostatic interactions.

Results and Discussion

Herein, the pyridyl cavitands **1** and the phenol cavitand **2** were used with various side chains (Figure 1; **a**: R = $(CH_2)_6CH_3$, **b**: R = $CH_2CH(CH_3)_2$, and **c**: R = $(CH_2)_3$-O-$CH_2CH[CH_2$-O-$(CH_2CH_2O)_3CH_3]_2$).

X-ray crystal structure of 3b@(1b·2b): Single crystals of **3b**@(**1b·2b**), suitable for X-ray diffraction analysis, were obtained by slow diffusion of benzene into a $CHCl_3$ solution of a 1:1:3 mixture of **1b**, **2b**, and **3b**. Two kinds of **3b**@(**1b·2b**) having slightly different conformations were found in the unit cell (Figures 2 and S2 in the Supporting Information).

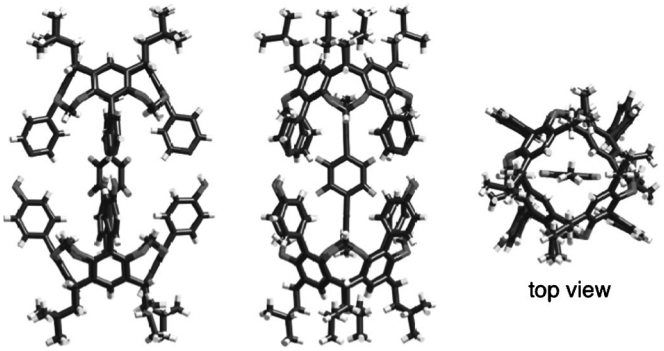

Figure 2. X-ray crystal structure of **3b**@(**1b·2b**): one of two slightly different conformers (occupancy factors of F1–F4 = 0.50) is shown.

The propynyl groups at the 1,4-positions of the encapsulated **3b** are oriented toward both aromatic cavity ends of **1b·2b**.

It is noteworthy that the cavity dimensions of **3b**@(**1b·2b**) are slightly, yet unambiguously, different from those of the previous reported **4c**@(**1b·2b**)[10c] and **5**@(**1b·2b**),[10b] with keeping average hydrogen-bonding distances between **1b** and **2b** almost constant (Table S2 in the Supporting Information). The molecular length of **3b** is 1.23 and 1.14 Å longer than those of **4c** and **5**, respectively. The polar dimension in **3b**@(**1b·2b**) is 0.21 and 0.12 Å longer than in **4c**@(**1b·2b**) and **5**@(**1b·2b**), respectively, whereas the equatorial dimension of the **1b** unit or the **2b** unit in **3b**@(**1b·2b**) is 0.20 and 0.18 or 0.19 and 0.16 Å shorter than those of the **1b** units or the **2b** units in **4c**@(**1b·2b**) and **5**@(**1b·2b**), respectively. Thus, **1b·2b** can adjust the cavity dimensions, depending on the guest size, shape, and/or functional group. In all cases, it is also noted that the equatorial dimension of the **1b** unit is 0.21–0.23 Å shorter than that of the **2b** unit.

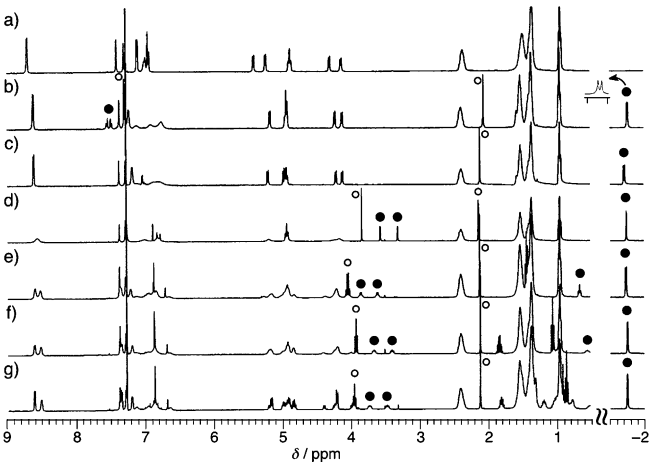

Figure 3. Association of heterocapsule **1a·2a** (5 mM) with guests **3** (10 mM) in $CDCl_3$ at 298 K monitored by ^{1}H NMR spectroscopy (400 MHz): a) **1a·2a** alone; b) **1a·2a**+**3a**; c) **1a·2a**+**3b**; d) **1a·2a**+**3c**; e) **1a·2a**+**3d**; f) **1a·2a**+**3e**; and g) **1a·2a**+**3f**. The representative signals for the encapsulated and free guests are marked with filled and open circles, respectively.

^{1}H NMR study: Association of heterocapsule 1a·2a with guests 3 in $CDCl_3$: The ^{1}H NMR spectra of **1a·2a** with **3** in $CDCl_3$ at 298 K are shown in Figure 3. The ^{1}H NMR signals of **3**@(**1a·2a**) and free **3** were independently observed and the signals of the encapsulated **3** appeared as two sets of signals, because the electronic environment of the **1** unit is different from that of the **2** unit, indicating that **3** does not tumble within **1a·2a** on the NMR time scale. The ^{1}H NMR signals of propynyl methyl protons of the encapsulated **3** were shifted largely upfield by 3.81–3.89 ppm relative to those of free **3** due to the ring-current effect of both the aromatic cavities of **1a·2a** (Table 1). These values were shifted more upfield by 0.3–0.4 ppm than those of the terminal methyl protons of **4**–**6**@(**1a·2a**).[10b,c] Because the association constants (K_a) of **1a·2a** with **3** were very large, comparison of the signal integrations between **3**@(**1a·2a**) and standard guest@(**1a·2a**), namely, competitive encapsulation experi-

Table 1. Association constants (K_a) and their free energies ($\Delta G°$) of heterocapsule **1a·2a** with guests **3**–**6** in $CDCl_3$ at 298 K, and ^{1}H NMR chemical-shift changes ($\Delta\delta$) of terminal methyl groups of encapsulated guests relative to free guests.

Guest	K_a [$\times 10^6$ M^{-1}][a]	$\Delta G°$ [kcal mol^{-1}][b]	$\Delta\delta$ [ppm][c]
3a	1140	−12.3	−3.82, −3.81
3b	520	−11.9	−3.89, −3.87
3c	163	−11.2	−3.87, −3.87
3d	275	−11.5	−3.85, −3.83
3e	45.4	−10.44	−3.86, −3.85
3f	42.7	−10.40	−3.85, −3.85
4a[d]	0.237	−7.41	−3.53, −3.50
4b[d]	1.07	−8.22	−3.51, −3.50
4c[d]	0.612	−7.89	−3.51, −3.41
5[e]	0.0812	−6.69	−3.43, −3.37
6[e]	0.0202	−5.87	−3.52, −3.47

[a] $K_a/K_{a-standard} = \{[G@(\mathbf{1a·2a})][G_{standard}]_f\}/\{[G_{standard}@(\mathbf{1a·2a})][G]_f\}$.
[b] $\Delta G° = -RT\ln K_a$. [c] $\Delta\delta = (\delta_{encapsulated\text{-}G} - \delta_{free\text{-}G})$. [d] See Ref. [10c]. [e] Ref. [10b].

ments, were used to estimate the K_a values of **1a·2a** with **3**.[10c,11,12] The K_a values of **1a·2a** with **3** in $CDCl_3$ at 298 K are summarized in Table 1.

The association of **1a·2a** with **3a** was found to be $K_a = 1.14 \times 10^9\,M^{-1}$ in $CDCl_3$ at 298 K. This K_a value is the largest among the guests investigated herein and is comparable to those of contiguous quadruple hydrogen-bonding arrays.[4] The K_a values of **1a·2a** with guests decreased in the order: **3a** > **3b** > **3d** > **3c** > **3e** > **3f** ≫ **4a** > **5** > **6**. Thus, the 1-propynyl group is the most favorable functional group among 1,4-disubstituted-benzene guests. The order of **3a–f@(1a·2a)** would be related to the steric hindrance between the alkoxy groups of **3c–f** and the equatorial walls of **1a·2a**. The ^{1}H NMR signals of the capsule moiety were extremely broadened in **3c–e@(1a·2a)** (Figure 3 d–f) or split in **3f@-(1a·2a)** (Figure 3 g) relative to those in **3a@(1a·2a)** and **3b@(1a·2a)** (Figure 3 b and c). This different behavior results from the slow rotation of the encapsulated **3c–e** along the long axis of **1a·2a** and from the inhibition of rotation for the encapsulated **3f** on the NMR time scale.[10c]

The observed association-free energy difference ($\Delta\Delta G° = -4.94$ kcal mol^{-1}) for the encapsulations of **3a** and **4a** in **1a·2a** was close to the theoretical calculation value of $\Delta\Delta G° = -4.56$ kcal mol^{-1} (see below). The ITC measurements for the association of **1a·2a** with **3a** showed $K_a = (1.75 \pm 0.39) \times 10^8\,M^{-1}$ in $CDCl_3$ at 298 K, and the thermodynamic parameters of enthalpy change $\Delta H° = -11.49 \pm 0.15$ kcal mol^{-1} and extremely small entropy change[2,13] $\Delta S° = -0.864 \pm 0.046$ cal mol^{-1} K^{-1} (Figure S11 in the Supporting Information).[14] Hence, the K_a value of **1a·2a** with **3a** estimated by the ^{1}H NMR competition experiments would be considered reasonable.

The encapsulation of **3** in **1a·2a** occurred instantaneously. However, once **3@(1a·2a)** is formed, the exchange of **3** in and out of **1a·2a** is too slow on the NMR time scale. In contrast to **4@(1a·2a)**,[10c] the exchange cross-peak between the encapsulated and free **3** in the 2D NOESY spectrum was not observed at 298 K, even at mixing time 1 s, and only marginally observed at 323 K (Figures S12–S17 in the Supporting Information). Thus, **3@(1a·2a)** is kinetically and thermodynamically much more stable than **4@(1a·2a)**. The guest exchanges between **3c@(1a·2a)** and **3a** and between **3a@(1a·2a)** and **3c** occurred on human time scale: it took 120 min to reach thermodynamic equilibration in $CDCl_3$ at 298 K (Figure 4).

Formation of 3a@(1·2a) in polar solvents: In general, hydrogen-bonded capsules dissociate upon addition of small amounts of polar solvents that compete for hydrogen-bond donors or acceptors.[7b] In polar solvents used in this work, **1a** and **2a** also exist as monomers instead of **1a·2a** in the absence of guests (Figure S18 in the Supporting Information). However, guests, such as **3a** and **4a**, induced the formation of **1a·2a**. The association of **1a** (hereafter, **1**),[15] **2a**, and guests obeys Equation (1). The exchange of free guest and guest@(**1·2a**) was slow on the NMR time scale even in the polar solvents (Figures 5 and S18–S28 in the Supporting Information). The results of K_{a2} (M^{-2}) in the polar solvents at 298 K are summarized in Table 2. As a reference, apparent association constants (K_{app}, M^{-1})[11a] according to Equation (2) are also summarized in Table S3 in the Supporting Information.

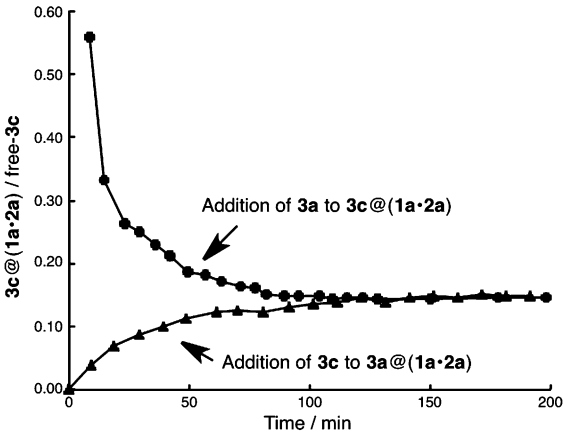

Figure 4. Plots of the ratio of the encapsulated **3c** to free **3c** (guest exchange ratio) in $CDCl_3$ at 298 K as a function of time (min), monitored by ^{1}H NMR spectroscopy, upon addition of **3a** (10 mM) to **3c@(1a·2a)** and free **3c** (5 mM each), and upon addition of **3c** (10 mM) to **3a@(1a·2a)** and free **3a** (5 mM each).

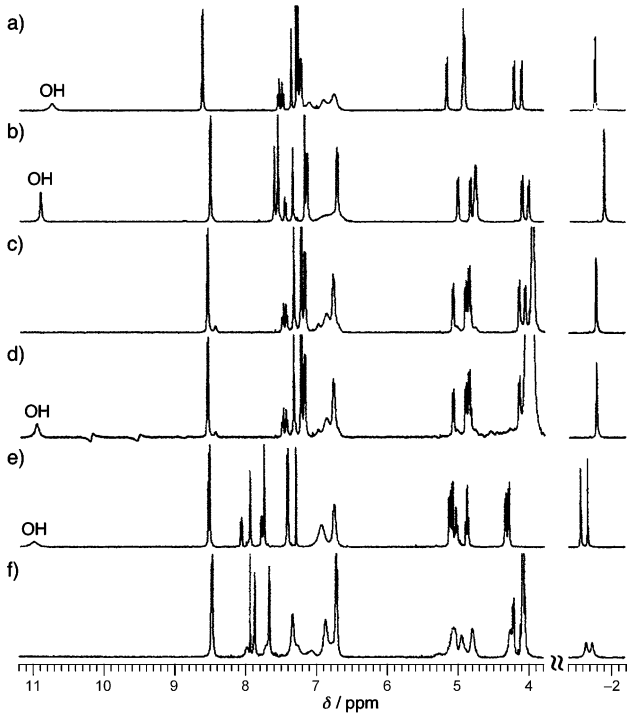

Figure 5. Association of **1**, **2a** (4 mM each), and **3a** (8 mM) in various solvents at 298 K monitored by ^{1}H NMR: a) **3a@(1a·2a)** in $CDCl_3$; b) **3a@-(1a·2a)** in [D_6]DMSO/$CDCl_3$ (20% v/v); c) **3a@(1a·2a)** in CD_3OD/$CDCl_3$ (20% v/v); d) **3a@(1a·2a)** in CH_3OH/$CDCl_3$ (20% v/v); e) **3a@-(1c·2a)** in [D_6]acetone; and f) **3a@(1c·2a)** in D_2O/[D_6]acetone (14.3% v/v).

Table 2. Association constants (K_{a2}) of **1a**, **2a**, and **3a**, or **4a** according to [Eq. (1)] and $\Delta G°_{(298\,K)}$ in polar solvents at 298 K, and their thermodynamic parameters ($\Delta H°$ and $\Delta S°$).

Guest	Solvent	K_{a2} $[M^{-2}]$[a]	$\Delta G°_{(298\,K)}$ [kcal mol^{-1}][b]	$\Delta H°$ [kcal mol^{-1}][c]	$\Delta S°$ [cal mol^{-1} K^{-1}][c]
3a	[D$_6$]DMSO/CDCl$_3$ (10% v/v)	6.32×10^{8}	−12.0	−16.2	−14.1
3a	[D$_6$]DMSO/CDCl$_3$ (15% v/v)	1.82×10^{8}	−11.3	−14.2	−9.96
3a	[D$_6$]DMSO/CDCl$_3$ (20% v/v)	2.58×10^{7}	−10.1	−11.2	−3.87
3a	[D$_6$]DMSO/CDCl$_3$ (25% v/v)	1.50×10^{7}	−9.79	−14.3	−15.0
3a	[D$_6$]DMSO/CDCl$_3$ (30% v/v)	6.35×10^{6}	−9.28	−14.8	−18.6
3a	[D$_6$]DMSO/CDCl$_3$ (40% v/v)	7.61×10^{5}	−8.02	−14.2	−20.6
3a	CD$_3$OD/CDCl$_3$ (10% v/v)	1.59×10^{8}	−11.2	−14.6	−11.5
3a	CD$_3$OD/CDCl$_3$ (15% v/v)	2.10×10^{7}	−9.98	−12.9	−9.72
3a	CD$_3$OD/CDCl$_3$ (20% v/v)	3.00×10^{6}	−8.83	−13.9	−16.9
3a	CD$_3$OD/CDCl$_3$ (25% v/v)	1.07×10^{6}	−8.22	−14.2	−19.9
3a	CD$_3$OD/CDCl$_3$ (30% v/v)	5.85×10^{5}	−7.86	−15.0	−23.7
3a	CD$_3$OD/CDCl$_3$ (35% v/v)	3.45×10^{5}	−7.55	−17.7	−33.8
3a[d,e]	[D$_6$]acetone	2.98×10^{9}	−12.9		
3a[d]	D$_2$O/[D$_6$]acetone (1.6% v/v)	9.19×10^{6}	−9.49		
3a[d]	D$_2$O/[D$_6$]acetone (14.3% v/v)	2.30×10^{5}	−7.31	−24.3	−57.0
3a[d]	D$_2$O/[D$_6$]acetone (25% v/v)	1.46×10^{5}	−7.04		
4a	[D$_6$]DMSO/CDCl$_3$ (10% v/v)	9.03×10^{5}	−8.12	−20.8	−42.8
4a	CD$_3$OD/CDCl$_3$ (10% v/v)	4.33×10^{4}	−6.32	−16.4	−33.8
4a[d]	[D$_6$]acetone	6.32×10^{6}	−9.27		
4a[d]	D$_2$O/[D$_6$]acetone (1.6% v/v)	1.16×10^{5}	−6.91		

[a] $K_{a2}=[\text{Guest@}(\mathbf{1a{\cdot}2a})]/\{[\mathbf{1a}]_f[\mathbf{2a}]_f[\text{Guest}]_f\}$ [Eq. (1)]. [b] $\Delta G°_{(298\,K)}=-298\,R\ln K_{a2}$. [c] $\Delta H°$ and $\Delta S°$ were obtained by van't Hoff plots: $\ln K_{a2}=-(\Delta H°/R)(1/T)+(\Delta S°/R)$. [d] Cavitand **1c** was used in place of **1a**. [e] Competitive formation of **3a**@(**1c·2a**) and **4a**@(**1c·2a**) was used to estimate the K_{a2} value.

$$K_{a2} = [\text{guest@}(\mathbf{1}\cdot\mathbf{2a})]/\{[\mathbf{1}]_f[\mathbf{2a}]_f[\text{guest}]_f\} \quad (1)$$

$$K_{app} = [\text{guest@}(\mathbf{1}\cdot\mathbf{2a})]/\{[\mathbf{1}\cdot\mathbf{2a}]_f[\text{guest}]_f\} \quad (2)$$

Addition of [D$_6$]DMSO as an aprotic polar solvent or CD$_3$OD as a protic polar solvent destabilized **3a**@(**1a·2a**) (Figures S19, S20, and S24a,b in the Supporting Information). However, the association constants still kept $K_{a2}=6.32\times10^{8}\,M^{-2}$ ($K_{app}=2.44\times10^{4}\,M^{-1}$) in 10% v/v [D$_6$]DMSO/CDCl$_3$ and $K_{a2}=1.59\times10^{8}\,M^{-2}$ ($K_{app}=1.17\times10^{4}\,M^{-1}$) in 10% v/v CD$_3$OD/CDCl$_3$.[16] The formation of **3a**@(**1c·2a**) also showed $K_{a2}=2.98\times10^{9}\,M^{-2}$ ($K_{app}=6.55\times10^{5}\,M^{-1}$) in [D$_6$]acetone and $K_{a2}=1.46\times10^{5}\,M^{-2}$ ($K_{app}=239\,M^{-1}$) in 25% v/v D$_2$O/[D$_6$]acetone (Figures S23 and S24c in the Supporting Information).[15] The thermodynamic stability of **3a**@(**1·2a**) decreased in the order of CDCl$_3$ ≫ [D$_6$]acetone > [D$_6$]DMSO/CDCl$_3$ ≥ CD$_3$OD/CDCl$_3$ > D$_2$O/[D$_6$]acetone. The $\Delta\Delta G°$ values for the formations of **3a**@(**1·2a**) and **4a**@(**1·2a**) at 298 K were $\Delta\Delta G°=-3.88$ kcal mol^{-1} in 10% v/v [D$_6$]DMSO/CDCl$_3$, $\Delta\Delta G°=-4.86$ kcal mol^{-1} in 10% v/v CD$_3$OD/CDCl$_3$, $\Delta\Delta G°=-3.65$ kcal mol^{-1} in [D$_6$]acetone, and $\Delta\Delta G°=-2.58$ kcal mol^{-1} in 1.6% v/v D$_2$O/[D$_6$]acetone (Table 2). It is thus understood how **3a** strongly stabilizes **1·2a** much more than **4a**.

The ^{1}H NMR OH signal of the phenol group in **3a**@(**1·2a**) appeared at $\delta=10.73$ in CDCl$_3$, 10.89 in 20% v/v [D$_6$]DMSO/CDCl$_3$, 10.89 even in 20% v/v CH$_3$OH/CDCl$_3$, and 11.00 ppm in [D$_6$]acetone (Figure 5). These chemical shifts remained almost unchanged in the range of at least 1–5 mM of **3a**@(**1·2a**), and in the range of 10–50% [D$_6$]DMSO/CDCl$_3$ (Figure S19 in the Supporting Information) and in the range of 10–35% CH$_3$OH/CDCl$_3$ (Figure S21 in the Supporting Information). These NMR results indicate hydrogen bonds in the capsule formation of **1** and **2a** with encapsulation of **3a**. Thus, the **3a**–**1·2a** interactions support the hydrogen bonds between **1** and **2a** in the polar solvents.

Thermodynamics of 3a@(1·2a) in polar solvents: As shown in Table 2 and Figures S29–S32 (van't Hoff plots) in the Supporting Information, in polar-solvent systems used in this work, the formations of **3a**@(**1·2a**) and **4a**@(**1·2a**) were enthalpically driven ($\Delta H°<0$ and $\Delta S°<0$), suggesting a nonclassical hydrophobic effect.[17]

There is a unique correlation between thermodynamic parameters in **3a**@(**1a·2a**) and polar solvents. In 10–40% v/v aprotic [D$_6$]DMSO/CDCl$_3$ (Figure 6a,c), there was a critical inflection point in the correlation between $\Delta H°$ versus $\Delta S°$ for the formation of **3a**@(**1a·2a**). For ≤20% [D$_6$]DMSO, with increasing amounts of [D$_6$]DMSO, the $\Delta H°$ and $\Delta S°$ contributions decreased and increased, respectively (but still kept $\Delta H°<0$ and $\Delta S°<0$), probably due to a contribution of the desolvation effect.[7b] Desolvated aprotic [D$_6$]DMSO would not hydrogen bond with bulk [D$_6$]DMSO molecules, leading to increase of the $\Delta S°$ contribution for the formation of **3a**@(**1a·2a**). On the other hand, for ≥20% [D$_6$]DMSO, with increasing amounts

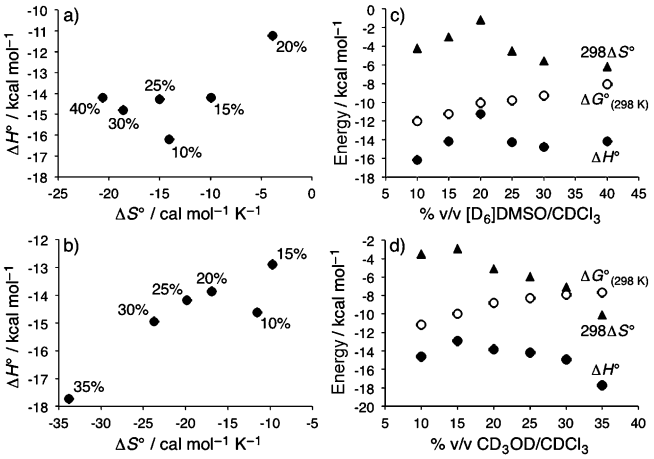

Figure 6. Correlations between thermodynamic parameters for the formation of **3a**@(**1a·2a**): plots of $\Delta H°$ versus $\Delta S°$ in a) [D$_6$]DMSO/CDCl$_3$ (10–40% v/v); and b) CD$_3$OD/CDCl$_3$ (10–35% v/v); plots of $\Delta H°$, $298\Delta S°$, and $\Delta G°_{(298\,K)}$ as a function of c) [D$_6$]DMSO content; and d) CD$_3$OD content.

of [D_6]DMSO, the $\Delta H°$ and $\Delta S°$ contributions increased and decreased, respectively, due to a nonclassical hydrophobic effect that is attributed mainly to a gain in the capsule–guest dispersion interactions.[17b] The results recorded in [D_6]DMSO/$CDCl_3$ suggest that the dispersion interaction of **1a·2a** with **3a** is inherently strong and effective. In 10–35% v/v protic CD_3OD/$CDCl_3$ (Figure 6b,d), there was an inflection point at 15% CD_3OD in the correlation between $\Delta H°$ versus $\Delta S°$. The $\Delta H°$ and $\Delta S°$ contributions also increased and decreased, respectively, with increasing amounts of CD_3OD. In this case, favorable changes in solvent cohesive interactions would be more important,[17,18] compared with [D_6]DMSO/$CDCl_3$. In both cases, the encapsulation process shows an enthalpy–entropy compensation effect.[17c]

Ab initio molecular-orbital calculations: Origin of the remarkable stability of 3a@(1·2): Previously, Tsuzuki et al. reported that ab initio calculation with the MP2 level electron-correlation correction is a very powerful tool for evaluating and studying the interaction energies for large systems, such as **1·2** complexes with guests.[19] The interaction energies were calculated for **3a**@(**1·2**) and **4a**@(**1·2**) at the MP2 level to elucidate the reasons for the remarkable stability of **3a**@(**1·2**) compared with **4a**@(**1·2**).[19–21] The computational method used in the present study followed that used in a previous report.[19] The geometries of guest@(**1·2**), guest free **1·2** (R = CH_3), and guests **3a** and **4a** were optimized at the HF/6-31G* level (Figure 7). The interaction energies were calculated by using the same basis set with the basis set superposition error (BSSE)[22] correction by the counterpoise method.[23] The calculated interaction energies between **1·2** and **3a** or **4a** and stabilization energies by formation of **3a**@(**1·2**) and **4a**@(**1·2**), and differences of each energy term (ΔE) between **3a**@(**1·2**) and **4a**@(**1·2**) are summarized in Table 3.[19,20] Details of energy terms are shown in footnote of Table 3.

Table 3. Interaction energy between heterocapsule **1·2** and guest **3a** or **4a**, stabilization energy (E_{form}) by formation of guest@(**1·2**), and difference of each energy term (ΔE) between **3a**@(**1·2**) and **4a**@(**1·2**).[a]

Guest@(**1·2**)	E_{int}[b,c]	E_{HF}[c,d]	E_{es}[e]	E_{rep}[f]	E_{corr}[g]	E_{def}[h]	E_{form}[i]
3a@(**1·2**)	−28.25	6.47	−9.15	15.62	−34.72	1.87	−26.38
4a@(**1·2**)	−25.82	4.82	−9.82	14.64	−30.64	4.00	−21.82
	ΔE_{int}	ΔE_{HF}	ΔE_{es}	ΔE_{rep}	ΔE_{corr}	ΔE_{def}	ΔE_{form}
3a@(**1·2**)−**4a**@(**1·2**)	−2.43	1.66	0.67	0.99	−4.09	−2.13	−4.56

[a] Energy [kcal mol^{-1}]. Geometries for **3a**@(**1·2**) and **4a**@(**1·2**) are shown in Figure 7. For detailed computational method, see Ref [19]. [b] Total interaction energy calculated at the MP2 level. $E_{int} = E_{HF} + E_{corr}$. [c] BSSE was corrected by the counterpoise method. [d] Interaction energy calculated at the HF level. [e] Electrostatic energy calculated as interactions between distributed multipoles of the interacting **1·2** and the guest. See Ref [19]. [f] $E_{rep} = E_{HF} - E_{es}$. E_{rep} is mainly exchange-repulsion energy. [g] Electron correlation contribution to total interaction energy. $E_{corr} = E_{int} - E_{HF}$. E_{corr} is mainly dispersion energy. [h] Sum of the increases of energies of **1·2** and guest by the deformation of molecular geometries associated with the formation of guest@(**1·2**), calculated at the HF/6-31G* level. [i] Stabilization energy by the formation of guest@(**1·2**) from an isolated **1·2** and a guest. $E_{form} = E_{int} + E_{def}$.

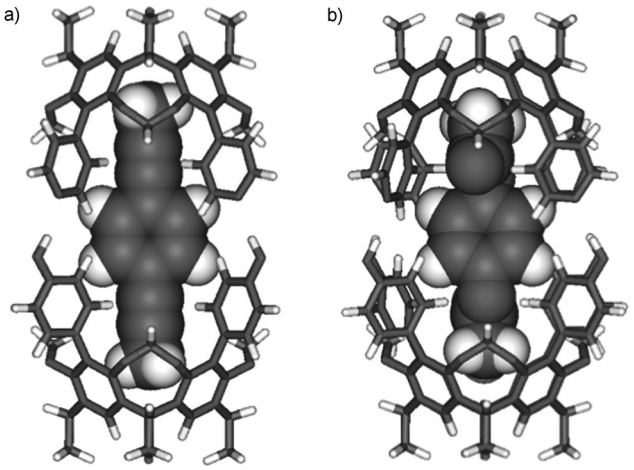

Figure 7. Geometries optimized for a) **3a**@(**1·2**); and b) **4a**@(**1·2**) calculated at the HF/6-31G* level.

The large negative electron-correlation contributions to the interaction energies (E_{corr}) compared with the electrostatic energies (E_{es}) show that the dispersion interactions are the major source of the attraction of **1·2** with guests in the gas phase. The large ΔE_{corr} (−4.09 kcal mol^{-1}) and small ΔE_{es} (0.67 kcal mol^{-1}) values indicate that larger dispersion interaction is mainly responsible for greater stability of **3a**@(**1·2**) compared with **4a**@(**1·2**). Thus, the difference of total interaction energy (ΔE_{int}) is −2.43 kcal mol^{-1}. Smaller deformation energy (E_{def}) is also an important source of greater stability of **3a**@(**1·2**). The ΔE_{def} is −2.13 kcal mol^{-1}. Therefore, the difference of the stabilization energies by the formation of the complexes from isolated **1·2** and guests ($\Delta E_{form} = \Delta E_{int} + \Delta E_{def}$) is −4.56 kcal mol^{-1}. This value well reproduces the experimentally observed thermodynamic free-energy difference of $\Delta\Delta G° = -4.94$ kcal mol^{-1} in $CDCl_3$ at 298 K. Thus, larger dispersion interaction between the 1-propynyl groups of **3a** and the aromatic inner space of **1·2** and less structural deformation of **1·2** upon encapsulation of **3a**, compared with those of **4a**@(**1·2**), play important roles in the remarkable stability of **3a**@(**1·2**).

The interactions of the acetylenic parts (triple bonds) of **3a** with **1** and **2** contribute largely to the strong attraction between **3a** and **1·2**. Intermolecular interaction energies (E_{int}) were calculated at the MP2/6-31G* level for the model complexes shown in Figure 8. The geometries of **3a**@**1** and **3a**@**2** were prepared from that of **3a**@(**1·2**) by removing **2** or **1**. The **7**@**1** and **7**@**2** (**7**: 2-butyne) are the models for evaluating the interactions of the methyl acetylenic parts of **3a** with **1** and **2**.[24] The **8**@**1** and **8**@**2** (**8**: methane) are the models for evaluating the interactions of the terminal methyl groups of **3a** with **1** and **2**.[24] The results

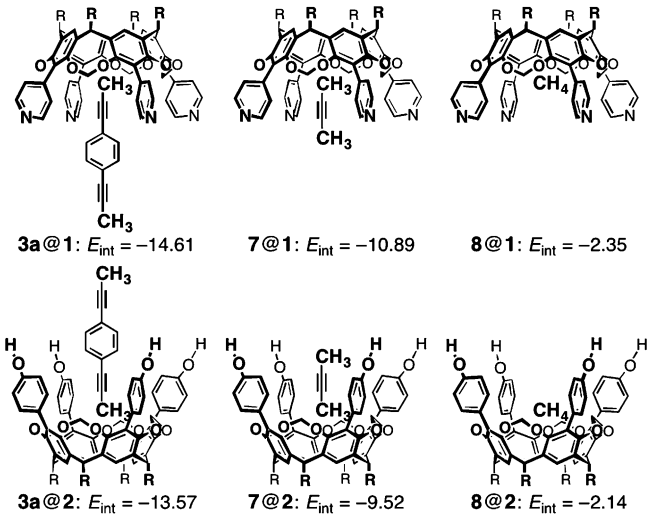

Figure 8. Interaction energies calculated for model complexes [kcal mol^{-1}].

are summarized in Table 4. The E_{int} calculated for **3a@1** and **3a@2** are −14.61 and −13.57 kcal mol^{-1}, respectively. They correspond to the interactions of **3a** with **1** and **2**, respectively. The E_{int} calculated for **7@1** and **7@2** are −10.89 and −9.52 kcal mol^{-1}, respectively. The sum of the E_{int} values is −20.41 kcal mol^{-1}, which is 72% of the E_{int} between **3a** and **1·2**. The E_{int} calculated for **8@1** and **8@2** are −2.35 and −2.14 kcal mol^{-1}, respectively. They are very weak in comparison with the interactions of **3a** with **1** and **2**, indicating that the interactions of the terminal methyl groups of **3a** with **1** and **2** do not play an important role in stabilizing **3a@1·2**, although the hydrogen atoms of the methyl groups have (CH/π) contacts with the aromatic cavity ends of **1** and **2**. These results show that the interactions of the acetylenic parts of **3a** with **1** and **2** have paramount importance for the strong attraction between **3a** and **1·2**.

Table 4. Interaction energy of **1** and **2** with guests **3a**, **7**, and **8**.[a]

Complex	E_{int}[b,c]	E_{HF}[c,d]	E_{es}[e]	E_{rep}[f]	E_{corr}[g]
3a@1	−14.61	4.42	−4.99	9.41	−19.03
3a@2	−13.57	2.13	−4.39	6.52	−15.70
7@1	−10.89	4.32	−4.44	8.76	−15.21
7@2	−9.52	3.13	−4.39	7.52	−12.65
8@1	−2.35	5.93	−0.14	6.07	−8.28
8@2	−2.14	5.73	−0.20	5.93	−7.87

[a] Energy [kcal mol^{-1}]; geometries are shown in Figure 8. [b–g] See footnotes [b–g] in Table 3.

The large attractive electrostatic interactions (E_{es} = −9.15 kcal mol^{-1}) were calculated for **3a@(1·2)**, as presented in Table 3. This shows that the electrostatic interaction is one of important sources for the strong attraction, although the attraction by the electrostatic interaction is weaker than the dispersion interaction. In **4a@(1·2)**, there are C=O···HC interactions between the carbonyl oxygen atoms of the acetoxy groups of **4a** and the inner protons of the methylene-bridge rims (O–CH_{in}H$_{out}$–O) of **1·2**[10c] to gain the E_{es}. There is no such interaction in **3a@(1·2)**. Nevertheless, the ΔE_{es} (0.67 kcal mol^{-1}) between **3a@(1·2)** and **4a@(1·2)** was relatively small. This would be attributed to a favorable electrostatic interaction between the acetylenic parts of **3a** and inner protons of the methylene-bridge rims of **1·2**. The E_{es} calculated for the model complexes support this idea. The E_{es} calculated for **7@1** and **7@2** are close to those for **3a@1** and **3a@2**, as shown in Table 4. The E_{es} calculated for **8@1** and **8@2** are very small. The calculations clearly show that the interactions of the acetylenic parts of **3a** with **1** and **2** are the origin of the large electrostatic interaction in **3a@(1·2)**. Hydrogen atoms of aromatic molecules have positive charges. The hydrogen atoms of pyridyl groups of **1** and phenol groups of **2** are close to the acetylenic part of **3a**. The hydrogen atoms of methylene-bridge rims of **1** and **2**, which have positive charge, are also close to the acetylenic parts of **3a**. The attractive electrostatic interactions of the acetylenic parts of **3a** with these positively charged hydrogen atoms are the source of the attractive electrostatic interactions.

Conclusion

The self-assembled hydrogen-bonded heterocapsule **1·2** can finely tune the cavity dimensions, depending on the nature of guest. We have demonstrated that the perfect match of dimensions, as well as *dispersion and electrostatic interactions of the acetylenic parts (triple bonds)* of **3a** with the aromatic inner space of **1·2** and the conformational rigidity of **3a** extraordinarily enhance the thermodynamic stability of **3a@(1·2)**. The **3a–1·2** interactions support the hydrogen bonds between **1** and **2** in polar solvents. We also found that there is an inflection point in the correlation between $\Delta H°$ versus $\Delta S°$ for the formation of **3a@(1·2)** as a function of polar-solvent content. The guest@(**1·2**) offers the great advantage that its thermodynamic stability is controlled by guests **3–6** in the range $K_a = 1\times10^9$–1×10^4 M^{-1} in $CDCl_3$ at 298 K. This implies that the unit of guest@(**1·2**) is a promising candidate as an *affinity-variable supramolecular synthon* for supramolecular architectures, such as supramolecular polymers.[1b,3,6a,b,25]

Experimental Section

General: ^{1}H and ^{13}C NMR spectra were recorded at 400 and 100 MHz, respectively, on a JEOL JNM-AL400 spectrometer. IR spectra were recorded on a JASCO FT/IR-460Plus spectrometer. High-resolution ESI-TOF-MS and EI-TOF-MS were performed on a JEOL JMS-T100LP and a JEOL JMS-T100GCV, respectively. The isothermal titration calorimetric (ITC) experiment was performed on a TA Instruments Nano-ITC 2G. Recycle preparative HPLC was performed on a Japan Analytical Industry LC-918 by using polystyrene gel columns (JAIGEL 1H and 2H) with $CHCl_3$ as an eluent. The $CDCl_3$ employed in all the ^{1}H NMR and ITC experiments was stored over K_2CO_3 prior to use, and the other NMR sol-

vents were used without any pretreatment. Tetra(4-pyridyl)-cavitands **1a**[26] and **1b**[10b] and tetrakis(4-hydroxyphenyl)-cavitands **2a**[10a] and **2b**[10b] (**a**: R = $(CH_2)_6CH_3$, **b**: R = $CH_2CH(CH_3)_2$) were synthesized according to the literature procedures. Synthetic procedures for **3a–f** are shown in the Supporting Information.

Synthesis of tetra(4-pyridyl)-cavitand with oligoether side chain (1c; Scheme 1): Under Ar, to a mixture of tetraiodo cavitand with oligoether side chain **9c** (375 mg, 0.13 mmol),[27] 4-pyridineboronic acid (198 mg,

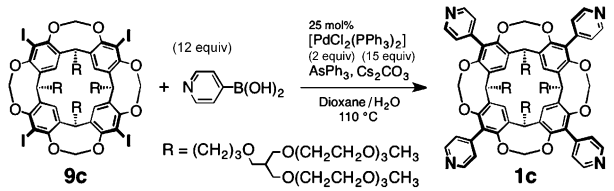

Scheme 1.

1.61 mmol), $[PdCl_2(PPh_3)_2]$ (24.0 mg, 0.034 mmol), $AsPh_3$ (79.6 mg, 0.26 mmol), and Cs_2CO_3 (655 mg, 2.01 mmol) were added 1,4-dioxane (14 mL) and H_2O (0.6 mL). This mixture was stirred at 110 °C for 48 h under Ar. After cooling to RT, the reaction mixture was filtered and washed with CH_2Cl_2 to remove Pd black. After evaporation of the filtrate, the residue was purified by column chromatography on silica gel eluted with EtOH/EtOAc (4:1) containing Et_3N (3% v/v). After evaporation of the fractions containing **1c**, the residue was dissolved in $CHCl_3$ and filtered to remove trace amount of silica gel. The evaporation of the filtrate gave **1c** as a pale yellow solid (146 mg, 46% yield). M.p.: 154 °C; ^{1}H NMR ($CDCl_3$): δ = 8.60 (d, J = 6.0 Hz, 8H), 7.36 (s, 4H), 6.97 (d, J = 6.0 Hz, 8H), 5.30 (d, J = 6.6 Hz, 4H), 4.94 (t, J = 7.8 Hz, 4H), 4.21 (d, J = 6.6 Hz, 4H), 3.65–3.48 (m, 128H), 3.37 (s, 24H), 2.47–2.40 (m, 8H), 2.24–2.18 (m, 4H), 1.78–1.69 ppm (m, 12H); ^{13}C NMR ($CDCl_3$): δ = 152.3, 149.5, 141.9, 138.4, 127.0, 124.9, 120.8, 100.4, 71.9, 70.59, 70.54, 70.50, 69.7, 69.4, 59.0, 40.2, 36.2, 27.3, 26.7 ppm; HRMS (ESI): m/z calcd for $C_{136}H_{204}N_4O_{44}+Na^+$: 2620.37461 [$M+Na^+$]; found: 2620.37236.

X-ray data collection and crystal-structure determination of 3b@(1b·2b): The data were recorded by using a Bruker APEXII CCD area detector, by using $Mo_{K\alpha}$ graphite monochromated radiation (λ = 0.71073 Å). The structure was solved by direct methods by using the program SHELXS-97.[28] The refinement and all further calculations were carried out by using SHELXL-97.[28] The hydrogen atoms were included in calculated positions and treated as riding atoms by using the SHELXL default parameters. The nonhydrogen atoms were refined anisotropically by using weighted full-matrix least-square method on F^2. Crystal data and structure refinement are listed in Table S1 in the Supporting Information, and ORTEP view is shown in Figure S2 in the Supporting Information. CCDC-893646 (3b@(1b.2b)) contains the supplementary crystallographic data for this paper. These data can be obtained free of charge from The Cambridge Crystallographic Data Centre via www.ccdc.cam.ac.uk/data_request/cif.

Acknowledgements

This work was supported in part by a Grant-in-Aid from JSPS (No. 22350060 (K.K.)) and Grant-in-Aid for Scientific Research on Innovative Areas "Emergence in Chemistry (K.K.)" and "Advanced Molecular Transformations by Organocatalysts (S.T.)" from MEXT.

[1] a) H.-J. Schneider, *Angew. Chem.* **2009**, *121*, 3982–4036; *Angew. Chem. Int. Ed.* **2009**, *48*, 3924–3977; b) T. F. A. de Greef, M. M. J. Smulders, M. Wolffs, A. P. H. J. Schenning, R. P. Sijbesma, E. W. Meijer, *Chem. Rev.* **2009**, *109*, 5687–5754 and references cited therein.

[2] For extraordinarily large K_a in a non hydrogen-bonded host-guest system, see: M. V. Rekharsky, T. Mori, C. Yang, Y. H. Ko, N. Selvapalam, H. Kim, D. Sobransingh, A. E. Kaifer, S. Liu, L. Isaacs, W. Chen, S. Moghaddam, M. K. Gilson, K. Kim, Y. Inoue, *Proc. Natl. Acad. Sci. USA* **2007**, *104*, 20737–20742.

[3] a) T. Haino, E. Hirai, Y. Fukazawa, K. Kashihara, *Angew. Chem.* **2010**, *122*, 8071–8075; *Angew. Chem. Int. Ed.* **2010**, *49*, 7899–7903; b) F. Tancini, R. M. Yebeutchou, L. Pirondini, R. De Zorzi, S. Geremia, O. A. Scherman, E. Dalcanale, *Chem. Eur. J.* **2010**, *16*, 14313–14321.

[4] a) F. H. Beijer, R. P. Sijbesma, H. Kooijman, A. L. Spek, E. W. Meijer, *J. Am. Chem. Soc.* **1998**, *120*, 6761–6769; b) G. B. W. L. Ligthart, H. Ohkawa, R. P. Sijbesma, E. W. Meijer, *J. Am. Chem. Soc.* **2005**, *127*, 810–811; c) T. Park, S. C. Zimmerman, S. Nakashima, *J. Am. Chem. Soc.* **2005**, *127*, 6520–6521; d) B. A. Blight, C. A. Hunter, D. A. Leigh, H. McNab, P. I. T. Thomson, *Nat. Chem.* **2011**, *3*, 246 and references cited therein.

[5] a) J. Rebek, Jr., *Acc. Chem. Res.* **2009**, *42*, 1660–1668; b) T. Schröder, S. N. Sahu, D. Anselmetti, J. Mattay, *Isr. J. Chem.* **2011**, *51*, 725–742.

[6] a) R. K. Castellano, D. M. Rudkevich, J. Rebek, Jr., *Proc. Natl. Acad. Sci. USA* **1997**, *94*, 7132–7137; b) R. K. Castellano, R. Clark, S. L. Craig, C. Nuckolls, J. Rebek, Jr., *Proc. Natl. Acad. Sci. USA* **2000**, *97*, 12418–12421; c) J. M. C. A. Kerckhoffs, M. G. J. ten Cate, M. A. Mateos-Timoneda, F. W. B. van Leeuwen, B. Snellink-Ruël, A. L. Spek, H. Kooijman, M. Crego-Calama, D. N. Reinhoudt, *J. Am. Chem. Soc.* **2005**, *127*, 12697–12708.

[7] a) S. Mecozzi, J. Rebek, Jr., *Chem. Eur. J.* **1998**, *4*, 1016–1022; b) T. Amaya, J. Rebek, Jr., *J. Am. Chem. Soc.* **2004**, *126*, 14149–14156; c) E. S. Barrett, T. J. Dale, J. Rebek, Jr., *J. Am. Chem. Soc.* **2007**, *129*, 8818–8824.

[8] a) K. Kobayashi, K. Ishii, S. Sakamoto, T. Shirasaka, K. Yamaguchi, *J. Am. Chem. Soc.* **2003**, *125*, 10615–10624; b) K. Kobayashi, K. Ishii, M. Yamanaka, *Chem. Eur. J.* **2005**, *11*, 4725–4734.

[9] a) E. Huerta, G. A. Metselaar, A. Fragoso, E. Santos, C. Bo, J. de Mendoza, *Angew. Chem.* **2007**, *119*, 206–209; *Angew. Chem. Int. Ed.* **2007**, *46*, 202–205; b) H. Dube, M. R. Ams, J. Rebek, Jr., *J. Am. Chem. Soc.* **2010**, *132*, 9984–9985.

[10] a) K. Kobayashi, R. Kitagawa, Y. Yamada, M. Yamanaka, T. Suematsu, Y. Sei, K. Yamaguchi, *J. Org. Chem.* **2007**, *72*, 3242–3246; b) H. Kitagawa, M. Kawahata, R. Kitagawa, Y. Yamada, M. Yamanaka, K. Yamaguchi, K. Kobayashi, *Tetrahedron* **2009**, *65*, 7234–7239; c) H. Kitagawa, Y. Kobori, M. Yamanaka, K. Yoza, K. Kobayashi, *Proc. Natl. Acad. Sci. USA* **2009**, *106*, 10444–10448.

[11] a) T. Martín, U. Obst, J. Rebek, Jr., *Science* **1998**, *281*, 1842–1845; b) B. W. Purse, S. M. Butterfield, P. Ballester, A. Shivanyuk, J. Rebek, Jr., *J. Org. Chem.* **2008**, *73*, 6480–6488.

[12] Because guest exchanges between **3**@(**1a·2a**) and standard guest@(**1a·2a**) in $CDCl_3$ at 298 K were very slow on the NMR time scale, a mixture of **1a·2a**, **3**, and a standard guest in a 1:2:n ratio (n = 2–5) in $CDCl_3$ was heated at 323 K for 4 h to reach thermodynamic equilibration in competitive encapsulation experiments before the measurements of K_a at 298 K. In the competitive encapsulation experiments, the following combinations were used: **4b** versus **3e**, **4b** versus **3f**, **3c** versus **3e**, **3c** versus **3f**, **3c** versus **3b**, **3a** versus **3b**, **3a** versus **3c**, **3a** versus **3d** (Figure S10 in the Supporting Information), **3a** versus **3e**, and **3a** versus **3f**.

[13] H. Zeng, R. S. Miller, R. A. Flowers II, B. Gong, *J. Am. Chem. Soc.* **2000**, *122*, 2635–2644.

[14] The K_a value determined by the ITC experiment was one order of magnitude smaller than that estimated by the ^{1}H NMR competition experiment. The reason is that the former measurement was conducted in 1/100 concentration compared with the latter, so the effect of H_2O content in $CDCl_3$ as a hydrogen-bonding inhibitor could not be ignored.

[15] In D_2O/[D_6]acetone, **1c** with oligoether side chains was used instead of **1a** (Figure 1) because of low solubility of **1a**.

[16] It is known that a Rebek's self-assembled cylindrical capsule very tightly encapsulates (*E*)-4,4′-dimethylstilbene with $K_{a2} = 9.0 \times 10^5\,M^{-2}$

in $CD_3OD/[D_{12}]$mesitylene (10% v/v) at 300 K.[7b] It is also known that a contiguous quadruple DDAA–AADD hydrogen-bonding array of ureidopyrimidone shows $K_a = 170\,M^{-1}$ in $[D_6]DMSO/CDCl_3$ (10% v/v) at 298 K.[4a] It is thus understood how **3a**@(**1a**·**2a**) is thermodynamically so stable.

[17] a) E. L. Piatnitski, R. A. Flowers II, K. Deshayes, *Chem. Eur. J.* **2000**, *6*, 999–1006; b) E. A. Meyer, R. K. Castellano, F. Diederich, *Angew. Chem.* **2003**, *115*, 1244–1287; *Angew. Chem. Int. Ed.* **2003**, *42*, 1210–1250; c) D. H. Leung, R. G. Bergman, K. N. Raymond, *J. Am. Chem. Soc.* **2008**, *130*, 2798–2805.

[18] Protic polar solvents with high cohesive interactions prefer to interact with bulk solvent molecules rather than to solvate the complementary apolar surfaces of host and guest molecules, namely, desolvation of host and guest molecules from surrounding protic polar solvent molecules and the resulting rearrangement of the hydrogen-bonding network with bulk solvent molecules would be a primary driving force for determining guest encapsulation. The substitution of less favorable dispersion interactions between protic polar solvent molecules and the complementary surfaces of the host and guest molecules by more favorable dispersion interactions between the hydrocarbon surfaces in the host–guest complex would also be a major contribution to the favorable enthalpic driving force in protic polar solvents. See Ref. [17].

[19] S. Tsuzuki, T. Uchimaru, M. Mikami, H. Kitagawa, K. Kobayashi, *J. Phys. Chem. B* **2010**, *114*, 5335–5341.

[20] a) C. Møller, M. S. Plesset, *Phys. Rev.* **1934**, *46*, 618–622; b) M. Head-Gordon, J. A. Pople, M. J. Frisch, *Chem. Phys. Lett.* **1988**, *153*, 503–506; c) S. Tsuzuki, A. Fujii, *Phys. Chem. Chem. Phys.* **2008**, *10*, 2584–2594.

[21] Gaussian 03, Revision D.01, M. J. Frisch, G. W. Trucks, H. B. Schlegel, G. E. Scuseria, M. A. Robb, J. R. Cheeseman, J. A. Montgomery, Jr., T. Vreven, K. N. Kudin, J. C. Burant, J. M. Millam, S. S. Iyengar, J. Tomasi, V. Barone, B. Mennucci, M. Cossi, G. Scalmani, N. Rega, G. A. Petersson, H. Nakatsuji, M. Hada, M. Ehara, K. Toyota, R. Fukuda, J. Hasegawa, M. Ishida, T. Nakajima, Y. Honda, O. Kitao, H. Nakai, M. Klene, X. Li, J. E. Knox, H. P. Hratchian, J. B. Cross, V. Bakken, C. Adamo, J. Jaramillo, R. Gomperts, R. E. Stratmann, O. Yazyev, A. J. Austin, R. Cammi, C. Pomelli, J. W. Ochterski, P. Y. Ayala, K. Morokuma, G. A. Voth, P. Salvador, J. J. Dannenberg, V. G. Zakrzewski, S. Dapprich, A. D. Daniels, M. C. Strain, O. Farkas, D. K. Malick, A. D. Rabuck, K. Raghavachari, J. B. Foresman, J. V. Ortiz, Q. Cui, A. G. Baboul, S. Clifford, J. Cioslowski, B. B. Stefanov, G. Liu, A. Liashenko, P. Piskorz, I. Komaromi, R. L. Martin, D. J. Fox, T. Keith, M. A. Al-Laham, C. Y. Peng, A. Nanayakkara, M. Challacombe, P. M. W. Gill, B. Johnson, W. Chen, M. W. Wong, C. Gonzalez, J. A. Pople, Gaussian, Inc., Wallingford CT, **2004**.

[22] B. J. Ransil, *J. Chem. Phys.* **1961**, *34*, 2109–2118.

[23] S. F. Boys, F. Bernardi, *Mol. Phys.* **1970**, *19*, 553–566.

[24] The positions of the atoms in **7** and **8** were taken from those in **3a**. The positions of hydrogen atoms, which were added in constructing **7** and **8**, were optimized at the HF/6-31G* level.

[25] a) A. Noro, Y. Matsushita, T. P. Lodge, *Macromolecules* **2008**, *41*, 5839–5844; b) A. Noro, H. Yamagishi, Y. Matsushita, *Macromolecules* **2009**, *42*, 6335–6338.

[26] K. Kobayashi, Y. Yamada, M. Yamanaka, Y. Sei, K. Yamaguchi, *J. Am. Chem. Soc.* **2004**, *126*, 13896–13897.

[27] L. Sebo, F. Diederich, V. Gramlich, *Helv. Chim. Acta* **2000**, *83*, 93–113.

[28] G. M. Sheldrick, *SHELXS-97* and *SHELXL-97*, University of Göttingen, Göttingen, Germany, **1997**.

Received: November 3, 2012
Published online: January 29, 2013

